Chemistry Europe
European Chemical Societies Publishing

Origin of Stability and Inhibition of Cooperative Alkyne Hydrofunctionalization Catalysts

Devon E. Chapple,[a] Paul D. Boyle,[a] and Johanna M. Blacquiere*[a]

New entries to the [Ru(Cp/Cp*)($P^R{}_2N^{R'}{}_2$)(MeCN)]PF_6 catalyst family were synthesized, including a Cp complex (R = Cy; R′ = Ph) and two Cp* complexes (R = Cy, Ph; R′ = Ph). These and other derivatives were used for the intramolecular hydroamination of 2-ethynylaniline to elucidate trends in catalytic lifetime and rate. The readily accessible [Ru(Cp)($P^{Cy}{}_2N^{Ph}{}_2$)(MeCN)]PF_6 derivative showed comparable lifetime to [Ru(Cp)($P^{t-Bu}{}_2N^{Ph}{}_2$)(MeCN)]PF_6, the previous optimal catalyst. Donor-free 'active' catalysts, [Ru(Cp/Cp*)($P^{Cy}{}_2N^{Ph}{}_2$)]PF_6, were prepared and their thermal stability was assessed. The relatively high stability of the Cp derivative was explained by the capacity of the $P^{Cy}{}_2N^{Ph}{}_2$ ligand to coordinate in a κ^3-(P,P,Ar) mode, which protects the low-coordinate species. This coordination mode is inaccessible with the Cp* derivative. Additionally, [Ru(Cp*)($P^{Cy}{}_2N^{Ph}{}_2$)]PF_6 readily activated the C–Cl bond of the solvent dichloromethane. Variable time normalization analysis (VTNA) revealed that the indole product inhibited the catalyst [Ru(Cp)($P^{Cy}{}_2N^{Ph}{}_2$)(MeCN)]PF_6, which slowed catalytic rates.

Introduction

Development and improvement of synthetic routes to nitrogen- and oxygen-containing heterocycles is valuable for the preparation of pharmaceutical drugs, agrochemicals, and natural products.[1] An atom-economic route to heterocycles is transition-metal catalyzed intramolecular hydrofunctionalization of alkynes.[2] Depending on the catalyst and substrate structure, alkyne activation by π-coordination can afford either the *exo-dig* or *endo-dig* products. Exclusive selectivity for the latter can be achieved with catalysts that activate the alkyne to give a metal vinylidene, in which the high electrophilicity of Cα directs nucleophilic attack to that site.[2a,b,3] In the case of ruthenium catalysts, the hydrofunctionalization mechanism[4] involves multiple proton transfer steps, which can be mediated by an exogenous base additive or solvent, such as pyridine.[5] Alternatively, additive-free methods are possible with cooperative[6] catalysts that contain a Brønsted base as part of a supporting ligand.[7]

We have systematically studied structure-performance relationships of [Ru(Cp/Cp*)($P^R{}_2N^{R'}{}_2$)(MeCN)]PF_6 (**1**, Cp; **2**, Cp*) catalysts that contain the cooperative $P^R{}_2N^{R'}{}_2$ (1,5-R′-3,7-R-1,5-diaza-3,7-diphosphacyclooctane) ligand (Figure 1a).[8] The pendent amine groups effectively promote proton transfer steps if the amine is moderately basic (i.e. R′ = Ph).[8a] Increased basicity with the stronger donor group R′ = benzyl leads to undesired vinylidene deactivation.[8b,9] Steric bulk in the primary coordination sphere with R < C => *t*-Bu, and Cp* as the spectator ligand (i.e. **2a**) promoted facile catalyst conscription, which involves dissociation of the placeholder MeCN ligand to give the on-cycle active catalyst (Figure 1b).[8c] This permitted hydrofunctionalization at moderate temperatures, but at the expense of lower catalyst lifetime as compared to a Cp catalyst analogue (**1a**). We hypothesized that the higher MeCN lability gives a higher proportion of the donor-free active catalyst, [Ru(Cp/Cp*)($P^R{}_2N^{R'}{}_2$)]PF_6, a likely vector for decomposition. Thus, understanding the factors that control stability of the active catalyst is of utmost importance to further increase catalyst lifetime.

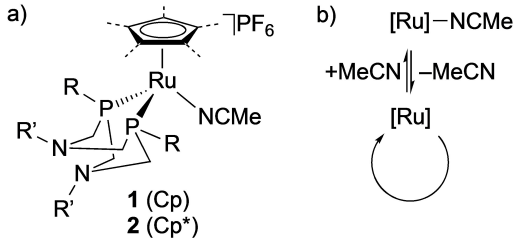

Figure 1. a) General structure of [Ru(Cp/Cp*)($P^R{}_2N^{R'}{}_2$)(MeCN)]PF_6 intramolecular hydrofunctionalization catalysts; and b) simplified depiction of catalyst conscription by MeCN dissociation to give the donor-free active catalyst.

The donor-free complex [Ru(Cp*)($P^{t-Bu}{}_2N^{Ph}{}_2$)]$BAr^F{}_4$ (**A**) was recently reported by Mock and co-workers as the active catalyst for ammonia oxidation to give N_2.[10] Two different isomers of **A** were characterized, which differed based on the coordination mode of the $P^{t-Bu}{}_2N^{Ph}{}_2$ ligand (Figure 2a). A low-coordinate isomer κ^2-(P,P)-**A** with a bidentate $P^{t-Bu}{}_2N^{Ph}{}_2$ mode was observed in both the solution and solid state. While the open site at the metal was not stabilized by any crystallographic close contacts, the boat conformation of the proximal metallocycle may offer steric protection. The second isomer κ^3-(P,P,N)-**A**, observed only in the solid-state, is stabilized by coordination of one of the pendent amine nitrogen atoms to ruthenium. Dynamic changes in the coordination mode of the $P^R{}_2N^{R'}{}_2$ ligand do occur in solution with Mn, Mo, Cr and Ni complexes,[11] which shows that

[a] D. E. Chapple, Dr. P. D. Boyle, Prof. J. M. Blacquiere
Department of Chemistry
Western University
1151 Richmond Street
London
Ontario, N6A 3K7 (Canada)
E-mail: johanna.blacquiere@uwo.ca

Supporting information for this article is available on the WWW under https://doi.org/10.1002/cctc.202100622

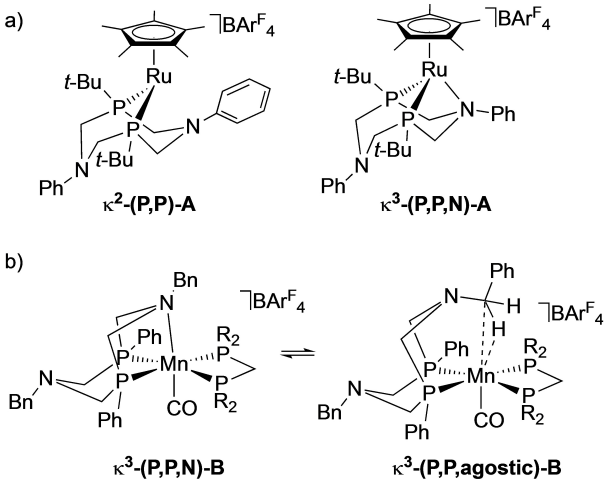

Figure 2. Versatile coordination chemistry of the $P^R{}_2N^{R'}{}_2$ ligand in donor-free a) ruthenium,[10] and b) manganese[11b] complexes.

the ligands are structurally responsive.[12] For example, a low-coordinate Mn(I) complex, **B**, is stabilized by two different tridentate modes κ^3-(P,P,N) and κ^3-(P,P,agostic), in which the latter includes agostic binding from the benzyl group of the pendent amine substituent (Figure 2b).[11b] The κ^3-(P,P,agostic) mode also stabilized $[Ni(P^{Ph}{}_2N^{Me}{}_2]^{2+}$ by ca. 5.5 kJ/mol relative to the more typical κ^2-(P,P) isomer.[11e] The capacity of the ligand to achieve the higher coordination number competed with substrate binding in electrocatalytic H_2 oxidation catalysis, which slowed catalytic rates.

Herein, we evaluate the generality of higher catalyst lifetime for Cp vs Cp* catalysts of the type $[Ru(Cp/Cp^*)(P^R{}_2N^{R'}{}_2)(MeCN)]PF_6$ toward intramolecular alkyne hydroamination. The structure and stability of the donor-free active catalysts is probed, which reveals the key role of $P^R{}_2N^{R'}{}_2$ ligand coordination mode on catalyst lifetime. Product inhibition is also identified as a dominant factor that influences catalytic rates.

Results and Discussion

Synthesis and Characterization of Catalysts **1b**, **2b**, and **2c**. The set of pre-catalysts (**1a–c**, **2a–c**) used in this study bear the phosphine substituents *t*-Bu, Cy or Ph (**a-c**, respectively) and an ancillary Cp (**1**) or Cp* (**2**) ligand (Figure 3). Complexes **1b**, **2b** and **2c** were not previously reported, but preparation by $P^R{}_2N^{R'}{}_2$ ligand coordination to $[Ru(Cp/Cp^*)(MeCN)_3]PF_6$ afforded the target complexes in excellent yields. The $^{31}P\{^1H\}$ NMR signals for **1b**, **2b**, and **2c** were observed at δ_P = 45.9, 36.0, and 33.4, respectively. The more upfield shift of the Cp* complex 2b as compared to the Cp analogue 1b is consistent with related derivatives[8c] and the difference reflects the greater donor strength of Cp*.

Single crystals of the R = Cy complex **2b** were obtained and X-ray crystallography confirmed the expected connectivity (Figure 4). The Ru(1)-P(1) and Ru(1)-P(2) bond distances were 2.275(2) and 2.262(2) Å, respectively, which were ca. 0.03–0.05 Å

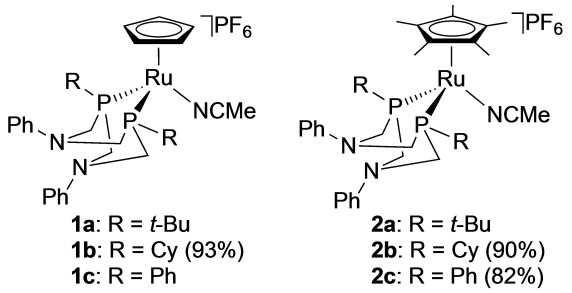

Figure 3. Cationic ruthenium complexes employed in this study. Yields for newly synthesized complexes shown in parentheses.

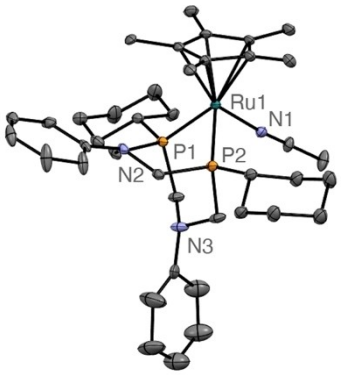

Figure 4. Displacement ellipsoid plot of complex **2b**. Ellipsoids are given at 30% probability level. H atoms, $[PF_6]^-$ anion, and a molecule of co-crystalized hexanes were omitted for clarity. Selected bond distances (Å): Ru(1)-N(1) = 2.046(4), Ru(1)-P(1) = 2.275(2), Ru(1)-P(2) = 2.262(2). Selected angles (°): P(1)-Ru(1)-P(2) = 78.80(5), Ru(1)-N(1)-C(1) = 175.1(4).

shorter than the analogous bond distances reported for the *t*-Bu analogue **2a**.[8c] The shorter distances for **2b** are a consequence of the greater flexibility and lower steric demand of the cyclohexyl substituents as compared to *t*-butyl. The different steric profile allows for slightly wider P(1)-Ru(1)-P(2) bite angle for **2b** (78.80(5)°) than **2a** (77.75(4)°).

Lifetime of Catalysts 1a-c and 2a–c.

The benchmark substrate 2-ethynylaniline (**EA**) was selected to evaluate the catalytic performance of **1b–c** and **2b–c** toward intramolecular hydroamination. The performance was compared directly to that of $P^{t-Bu}{}_2N^{Ph}{}_2$ catalysts **1a** and **2a**, which we reported previously.[8c] Reactions were conducted in Me-THF with a 0.1 mol% catalyst loading (Scheme 1). An elevated temperature of 70 °C was selected to ensure facile MeCN lability so that differences in catalyst initiation have limited impact on the observed activity. All catalytic reactions were monitored over time and the turnover number (TON) was determined at 24 h or once the catalyst conversion reached a plateau (Figure 5).

For each of the three $P^R{}_2N^{Ph}{}_2$ ligands, the Cp catalysts (**1**) gave superior TONs than the Cp* derivatives (**2**). The difference

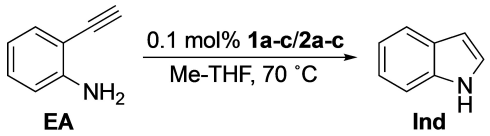

Scheme 1. General conditions for the intramolecular hydroamination of **EA** with Ru catalysts **1a–c** and **2a–c**.

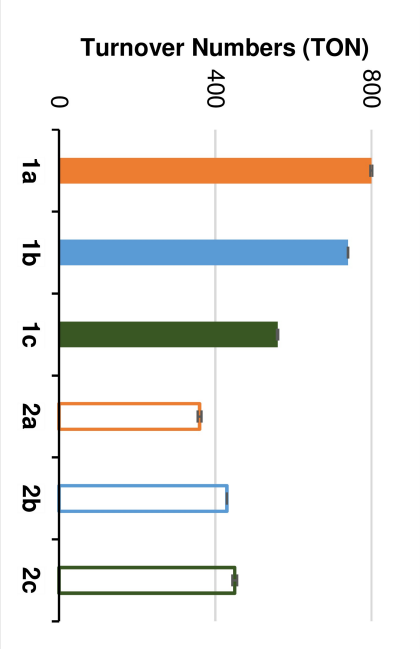

Figure 5. Turnover numbers (TON) of Cp (solid bars) and Cp* (empty bars) catalysts for intramolecular hydroamination of **EA**. Reaction conditions: 300 mM **EA**, Me-THF, 70 °C, 0.1 mol% [Ru]. Catalysts with R = *t*-Bu (orange), R = Cy (blue), and R = Ph (green). Runs were conducted in duplicate with data points representing the average and the error bars depict the span of individual runs.

was most notable for R = *t*-Bu (**1a**, **2a**) and R = Cy (**1b**, **2b**) in which the Cp catalysts exhibited TONs that were 2.2 and 1.7 times higher than the Cp* versions, respectively. In contrast, the TONs for R = Ph catalyst **1c** are only ca. 1.2 times higher than **2c**. While this confirms the previous observation with **1a**/**2a** that the TON is enhanced for Cp vs Cp* derivatives, the magnitude of the difference is dependent on the nature of the R group. The TONs for the Cp catalysts **1a-c** were 800, 740 and 560, respectively, giving a performance trend in phosphine substituent (R) of *t*-Bu > Cy > Ph. This trend reasonably tracks with steric properties as judged by %buried volumes (%V_{bur}) of AuCl(PR_3) complexes (38.1, 33.4 and 29.9 % for R = *t*-Bu, Cy and Ph, respectively, for M-P = 2.28 Å).[13] The trend in TONs for **1a-c** could also be consistent with the donor strength of the phosphine, in which the catalysts with the stronger donors **1a** and **1b** are superior to **1c**. It is notable, that an R = Bn catalyst exhibited very poor activity at 55 °C as compared to R = *t*-Bu or Ph,[8c] which suggests that either steric properties dominate or that the benzyl derivative was highly sensitive to a competing decomposition pathway. The performance trend of phosphine donor substituent is different for the Cp* catalysts, in which the TONs are similar for all derivatives (**2a** = 360; **2b** = 430; **2c** = 450). We proposed that the greater sensitivity of the Cp* catalysts to decomposition (*vide infra*) overrides any discernible difference in phosphine donor properties. The above studies indicate that catalysts **1a** and **1b** have similar TONs and are the longest lived of the derivatives studied. From a practical perspective, catalyst **1b** (R = Cy) is preferred over **1a** (R = *t*-Bu) due to the more amenable synthesis of the $P^{Cy}{}_2N^{Ph}{}_2$ ligand that includes both higher synthetic yields and a more economical phosphine precursor (i.e. by ca. 10-fold).[14]

Preparation of Hydroamination Active Catalysts.

Previously, we proposed that the lower lifetime of the Cp* catalyst **2a** vs the Cp derivative **1a** was due to decomposition of the active catalyst, which is more accessible for the former as a consequence of higher MeCN lability.[8c] The successful synthesis of **A**[10] indicates that the active complexes of **1b** and **2b** should also be synthetically accessible, which would permit direct stability assessment. To this end, we first synthesized the precursor chloro complexes [RuCl(Cp/Cp*)($P^{Cy}{}_2N^{Ph}{}_2$)] (**3b**, Cp; **4b**, Cp*) in very good yields (86 and 86 %, respectively) by ligand substitution with [RuCl(Cp/Cp*)(PPh_3)$_2$]. The $^{31}P\{^1H\}$ NMR signals corresponding to **3b** and **4b** were observed at δ_P = 46.6 and 34.4, respectively. Single crystals of both complexes were obtained, and X-ray crystallography confirmed the expected connectivity (Figure 6). Similar Ru–Cl bond distances were observed for **3b** and **4b** of 2.4556(6) and 2.459(2) Å, respectively. The Ru–P distances were longer for the Cp complex than Cp* by only ca. 0.02 Å. A slightly smaller P–Ru-P bite angle of 79.20(2)° was observed for **3b** as compared to 80.25(3)° for **4b**.

Halide abstraction from **3b** and **4b** gives operationally unsaturated products **5b-N_2** and **6b-N_2**, respectively, that are stabilized by a weakly coordinated N_2 ligand (Scheme 2). In addition, abstraction from the Cp derivative **3b** also affords a

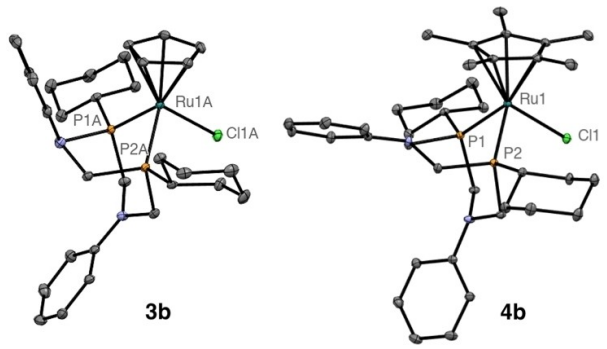

Figure 6. Displacement ellipsoid plot of solid-state structures of chloro complexes **3b** and **4b** with ellipsoids at 30 % probability level. H atoms and a molecule of co-crystalized DCM in **3b** were omitted for clarity. Selected bond distances (Å): **3b**, Ru(1)-Cl(1) = 2.4556(6), Ru(1)-P(1) = 2.2616(6), Ru(1)-P(2) = 2.2570(8); **4b**, Ru(1 A)-Cl(1 A) = 2.459(2), Ru(1 A)-P(1 A) = 2.244(1), Ru-(1 A)-P(2 A) = 2.277(1). Selected Angles (°): **3b**, P(1)-Ru(1)-P(2) = 79.20(2); **4b**, P(1 A)-Ru(1 A)-P(2 A) = 80.25(3).

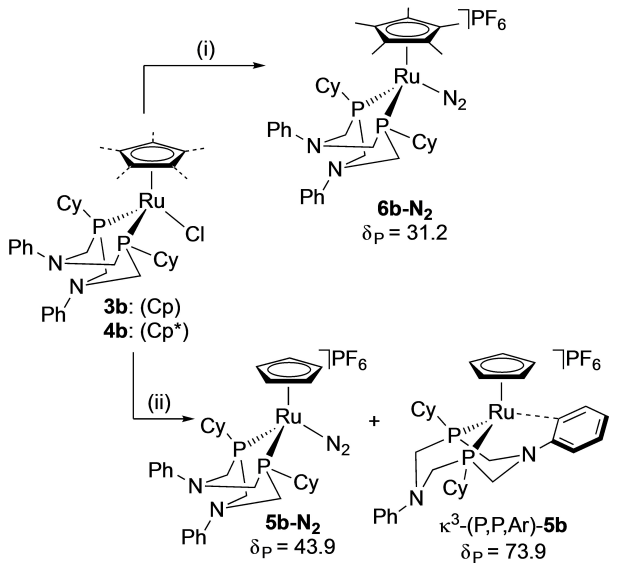

Scheme 2. Halide abstraction under N_2 utilizing $TlPF_6$ to generate complexes **5b-N$_2$** and **κ^3-(P,P,Ar)-5b**, and **6b-N$_2$** at room temperature in DCM and C_6H_5F, respectively.

product stabilized by a tridentate coordination of the $P^{Cy}{}_2N^{Ph}{}_2$ ligand. Characterization of the simpler case of the Cp* complex **6b-N$_2$** will be discussed first. Halide abstraction from **4b** resulted in a colour change from yellow to dark red, which is consistent with the formation of an operationally unsaturated[15] product. The ^{1}H NMR spectrum exhibited one signal for the methyl groups of the Cp* ligand, concordant with the expected η^5-coordination mode. None of the $P^{Cy}{}_2N^{Ph}{}_2$ ligand ^{1}H or ^{13}C resonances were shifted from the typical ranges found in κ^2-(P,P) complexes **2b** and **4b**. Analysis of the $^{31}P\{^1H\}$ NMR spectrum of **6b** revealed a new singlet at $\delta_P = 31.2$, which is 4.2 ppm upfield of that for **4b**. The location is consistent with that observed for **κ^2-(P,P)-A**, which exhibited a $^{31}P\{^1H\}$ resonance 5.5 ppm upfield of the neutral chloro complex **2a**.[10] However, the IR spectrum of **6b-N$_2$** showed a weak signal at $\nu = 2160\ cm^{-1}$ that is in the range expected for a N≡N stretch of a terminal Ru-N_2 adduct.[16] Treatment of **6b** with MeCN resulted in quantitative conversion to **2b** within five minutes, as judged by both $^{31}P\{^1H\}$ NMR analysis and the near instantaneous colour change from red to yellow. This suggests that the N_2 ligand is labile in solution and readily gives access to the low-coordinate 'active' complex. Attempts to obtain X-ray quality crystals of **6b-N$_2$** were unsuccessful.

Halide abstraction from **3b** resulted in a colour change from yellow to orange and the formation of two new singlets in the $^{31}P\{^1H\}$ NMR spectrum at 73.9 and 43.9 ppm. The ratio of the two compounds was variable, which could be a consequence of minor temperature fluctuations and instability of the more upfield species (*vide infra*). Addition of MeCN to the mixture rapidly gave quantitative formation of **1b**, which confirms that both products are operationally unsaturated. The signal at 43.9 ppm is ca. 2 ppm upfield of that for **3b**, which is consistent with an N_2 adduct, **5b-N$_2$**, analogous to **6b-N$_2$**. The dramatic ca. 30 ppm more downfield shift of the second species is indicative of a difference in chelation of the $P^{Cy}{}_2N^{Ph}{}_2$ ligand from κ^2-(P,P) to a tridentate mode that forms two 5- or 6-membered metallocycles.[17] The ^{1}H–^{13}C HSQC spectrum revealed a correlation between an aromatic proton to a ^{13}C signal at 95.8 ppm, a chemical shift that is expected for an aryl carbon engaged in metal coordination via the π-system.[18] This data suggests that the ruthenium centre in the downfield isomer of **5b** is stabilized via a κ^3-(P,P,Ar) coordination mode of the $P^{Cy}{}_2N^{Ph}{}_2$ ligand. Similar, π-coordination of a ligand aryl substituent is observed in palladium catalysts with dialkyl(biphenyl)phosphine ligands developed extensively by the Buchwald group.[12,19] Stabilization of Pd via reversible ligand coordination between κ^2-(P,Ar) and κ^1-(P) modes allows for exceptional turnover numbers in Suzuki C–C and Buchwald-Hartwig C–N coupling catalysis.

Single crystals suitable for X-ray diffraction were obtained from a sample containing >95% **κ^3-(P,P,Ar)-5b**, and the structure confirmed coordination of ruthenium to the *N*-phenyl substituent (Figure 7). A ruthenium pyramidalization angle ($Cp_{centroid}$-Ru-$PP_{centroid}$)[15a] of 144.49° strongly supports the presence of a stabilizing interaction in the sixth coordination site. The Ru(1)-C(15) distance of 2.429(2) Å is within the range (2.26–2.46 Å) observed for similar structures with Ru(II) coordination to the π-system of an aryl group.[16b,18c, 20] By contrast, the closest distance between Ru and an ortho carbon in **κ^2-(P,P)-A** is nearly 0.2 Å longer.[10] The capacity of the phenyl group to bind to ruthenium in **κ^3-(P,P,Ar)-5b**, is likely due to the small size of the Cp spectator ligand. In line with this hypothesis, complexes **A** and **6b** with the bulkier Cp* ligand, do not exhibit this

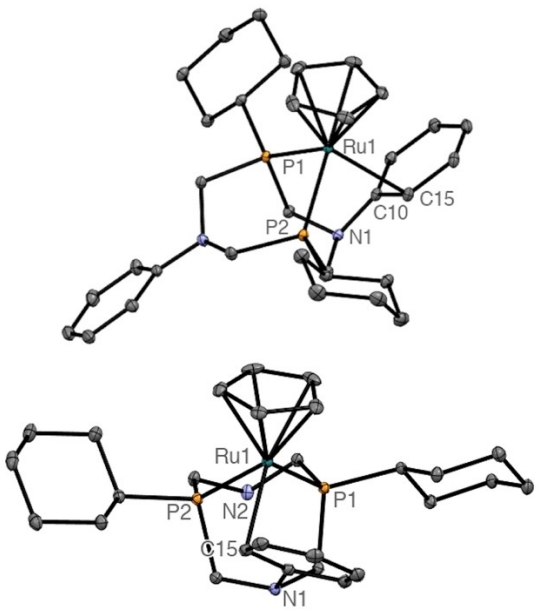

Figure 7. Two views of the displacement ellipsoid plots for **κ^3-(P,P,Ar)-5b** with ellipsoids at 30% probability level. H atoms, $[PF_6]^-$, and a molecule of co-crystalized DCM were omitted for clarity. In the bottom view, the N(2) phenyl substituent was also removed for clarity. Selected bond distances (Å): Ru(1)-Cl(10) = 2.572(2) Ru(1)-C(15) = 2.429(2), Ru(1)-P(1) = 2.2571(8), Ru(1)-P-(2) = 2.293(1); Selected Angles (°): P(1)-Ru(1)-P(2) = 81.23(2), Cp(centroid)-Ru(1)-P(centroid) = 144.49°.

coordination mode. Indeed, this is the first example of this coordination mode with metal complexes of the $P^{R}_2N^{R'}_2$ ligand family.

Efforts to study the equilibrium between **5b-N$_2$** and **κ^3-(P,P,Ar)-5b** by variable temperature studies were hindered by competing decomposition. Instead, the structures and energetics were validated through computational modelling. Vibrational frequency calculations indicated that the 'active' complexes **κ^2-(P,P)-5b**, **κ^3-(P,P,Ar)-5b**, and **5b-N$_2$** are all ground state species (Figure 8). Relative to the 16e$^-$ low-coordinate species, the κ^3-(P,P,Ar) isomer and N_2 adduct are both more stable by 47.7 and 74.5 kJ/mol, respectively. Analogous calculations with the Cp* complex **6b** revealed that a κ^3-(P,P,Ar) isomer is 63.0 kJ/mol less stable than the κ^2-P,P 16e$^-$ complex. This is likely due to steric clash of the Cp* methyl groups with the aryl that would be engaged in metal binding. The high energy of this isomer is consistent with experiments that show no evidence for this compound. Complex **6b-N$_2$** was only slightly more stable (ΔG = −5.8 kJ/mol) than the 16e$^-$ complex κ^2-(P,P)-**6b**, which is in line with experimental indicators that the N_2 ligand is very labile.

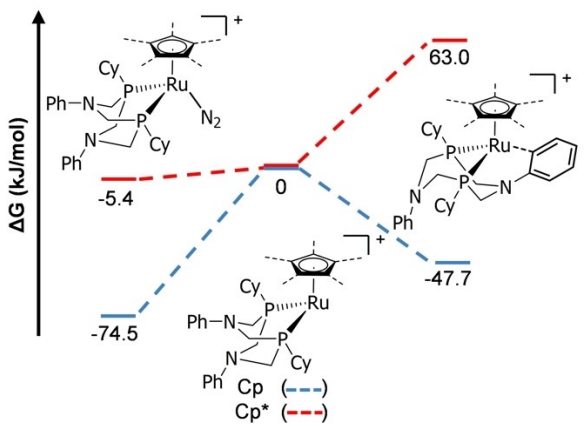

Figure 8. Calculated energies of 'active' catalyst cations of **5b** (blue) and **6b** (red) including N_2 adducts (left), low-coordinate κ^2-(P,P) (middle) and κ^3-(P,P,Ar) (right) isomers. The B3LYP/def2-SVP method was applied to all atoms except Ru, to which the B3LYP/def2-TZVP method with an ECP applied. The red dotted lines correspond to the energies for the Cp* (C_5Me_5) derivatives and the blue lines correspond to the energies of the Cp derivatives (C_5H_5).

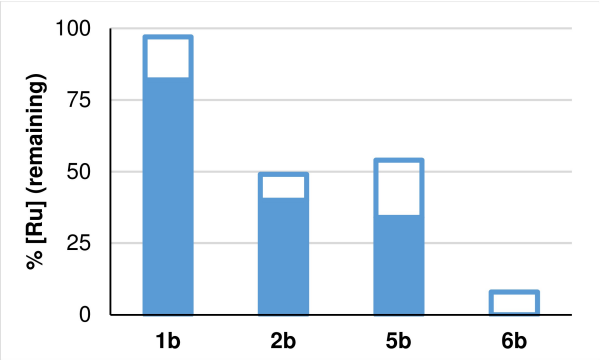

Figure 9. Thermal stability of pre-catalysts **1b/2b** and active catalysts **5b/6b** after 1 h (filled and empty bar together) and 24 h (filled bar only). %[Ru] values were quantified by $^{31}P\{^1H\}$ NMR spectroscopy integrals relative to an internal standard.

(In)Stability of Pre-Catalysts and Active Catalysts at Elevated Temperature

The thermal stability of pre-catalysts **1b/2b** and active catalysts **5b/6b** was assessed in nitromethane at 70 °C (Figure 9), which is the temperature used in catalytic reactions. Most conventional solvents were precluded for this assessment due to limited solubility of **5b** and **6b**, as well as competing reactivity with chlorinated solvents (*vide infra*) and competing adduct formation with coordinating solvents. As expected, the pre-catalysts **1b/2b** were more stable than the active catalysts analogues **5b/6b**. The Cp pre-catalyst **1b** is the most stable structure as is evidenced by 97 and 82% fidelity of speciation at 1 and 24 h, respectively. By contrast the active catalyst **5b** is ca. two-fold less stable in which only 54 and 34% of the complex remains at 1 and 24 h, respectively. The speciation of remaining **5b** at 70 °C is exclusively the κ^3-(P,P,Ar) isomer, which indicates the N_2 adduct with κ^2-(P,P) ligand coordination is more sensitive to decomposition. The Cp* pre-catalyst **2b** is ca. six-fold more stable than the active complex **6b**, however both are much less stable than the Cp analogues. Only 54% of the Cp* pre-catalyst **2b** remains after 1 h, which is similar stability to the Cp active catalyst **5b** (49% at 1 h). Strikingly, less than 10% of the Cp* active catalyst **6b** survives in the same timeframe. These data demonstrate that the Cp complexes are significantly more stable at elevated temperatures than the Cp* catalysts. We established previously with $[Ru(Cp/Cp^*)(P^{Ph}_2N^{Bn}_2)(MeCN)]PF_6$ complexes that MeCN is less labile with Cp as the ancillary ligand as compared to Cp*.[8c] The lower lability in **1b** would give a lower concentration of the more thermally sensitive active catalyst than **2b**. While this likely has some contribution to the relative thermal stability of **1b** and **2b**, the thermal stability of the active catalysts reveals that the Cp* derivative **6b** is intrinsically more sensitive to decomposition than the Cp derivative **5b**. We propose that the capacity for the $P^{Cy}_2N^{Ph}_2$ ligand in **5b** to achieve a κ^3-(P,P,Ar) coordination mode stabilizes the active catalyst from decomposition via the five-coordinate κ^2-(P,P) isomer. The thermolysis reactions resulted in the formation of multiple deactivation species (**5b** and **6b**) or the products were non-observable (**1b** and **2b**). In all cases, attempts to isolate the decomposition products proved unsuccessful.

(In)Stability of the Active Catalysts in Halogenated Solvent

Solutions of Cp* complex **6b-N$_2$** in CH_2Cl_2 (or CD_2Cl_2) cleanly converted to a single new compound at 70 °C after 1 h or at room temperature after 18 h (Scheme 3). By contrast, the Cp analogue **5b-N$_2$** was stable in CH_2Cl_2 over 48 h at room temperature. The product of **6b-N$_2$** decomposition was isolated in 90% yield and identified as **7**, which formed by cleavage of a C–Cl bond of the solvent to give a Ru–Cl moiety and a

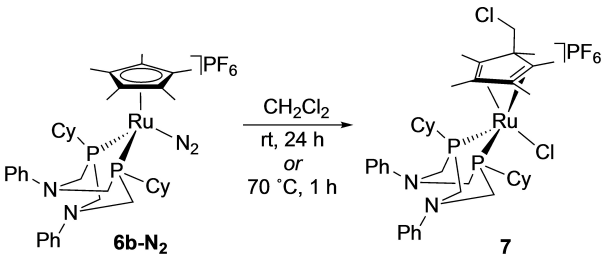

Scheme 3. Deactivation of operationally unsaturated complex **6b-N$_2$** via reaction with DCM to give Ru–Cl complex **7**.

functionalized cyclopentadiene ligand. The product was identified by two doublets in the $^{31}P\{^1H\}$ NMR spectrum at 72.5 and 32.8 ppm, which reflects the lack of symmetry. In the ^1H NMR spectrum a diagnostic signal for the Cp* methyl groups was absent, and instead four singlets were observed around 2 ppm and a fifth was found at 0.8 ppm. The upfield shift of the latter is a consequence of functionalization of one of the carbon atoms of the former Cp* ligand to give a cyclopentadiene structure. A similar pattern was found in the $^{13}C\{^1H\}$ NMR spectrum that contained four vinylic methyl signals around 12 ppm and one methyl bound to a *sp^3* carbon at 2.0 ppm. The functionalized quaternary carbon of δ_C = 1.32, is ca. 9 ppm upfield of the ring carbons of the Cp* ligand in **6b**. A correlation between this carbon and methylene protons at 3.55 and 3.28 ppm in the ^1H–^{13}C HMBC confirmed that the diene is functionalized with a 'CH$_2$Cl' unit originating from the solvent.

Single crystals of **7** were obtained and X-ray crystallography unambiguously confirmed the connectivity (Figure 10). The C(1 A) atom bears four substituents including the 'CH$_2$Cl' unit from the activated dichloromethane molecule. The C(1 A)-C(2 A) and C(1 A)-C(5 A) bond lengths are 1.529 and 1.532 Å, respectively, which are consistent with single bonds. Together, this confirms that the aromaticity of the ring has been broken. The cyclopentadiene ring is bound in an η^4-coordination mode, in which the Ru(1 A) to C(2 A)-C(5 A) bond lengths are 2.166(2), 2.222(2), 2.339(2), and 2.328(2) Å, respectively. The ca. 0.1 Å shorter distance to C(2 A) and C(3 A) reflects the stronger backbonding into the alkene trans to the π-donor chloride. The ruthenium centre is pseudo square pyramidal, in which phosphine P(2 A) of the $P^{Cy}{}_2N^{Ph}{}_2$ ligand occupies the axial site. This position *trans* to an open coordination site explains the ca. 40 ppm more downfield location of one of the $^{31}P\{^1H\}$ signals.

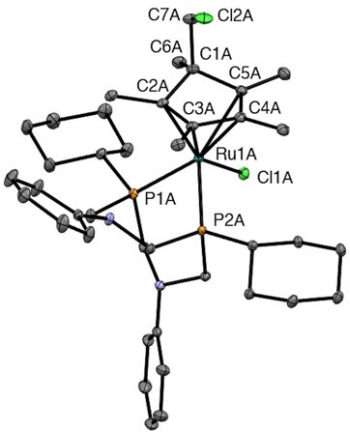

Figure 10. Displacement ellipsoid plot view of solid-state structure of [RuCl(η^4-C$_5$Me$_5$CH$_2$Cl)(P$^{Cy}{}_2$N$^{Ph}{}_2$)][PF$_6$] (**7**). Ellipsoids are given at 30% probability level. H atoms, [PF$_6$]$^-$ counterion, a molecule of co-crystalized CH$_2$Cl$_2$, and a minor component of disorder in the C$_5$Me$_5$CH$_2$Cl ligand were omitted for clarity. Selected bond distances (Å): Ru(1 A)-Cl(1 A) = 2.364(1), Ru(1 A)-P(1 A) = 2.2989(8), Ru(1 A)-P(2 A) = 2.2421(8). Selected Angles (°): P(1 A)-Ru(1 A)-P(2 A) = 77.31(2).

Oxidative addition of the C–Cl bond of dichloromethane is known for other Ru complexes bearing Cp* or Tp ancillary ligands (Tp = hydridotris(pyrazolyl)borate).[21] A similar reaction may occur en route to **7**, but no high-valent intermediates were observed. Certainly, the formation of **7** from **6b** would not be concerted since the Ru–Cl and 'CH$_2$Cl' fragments are on opposite faces of the cyclopentadiene ligand. Functionalization of Ru-bound Cp/Cp* ligands can occur via nucleophilic or electrophilic addition.[22] Regardless of the mechanism for CH$_2$Cl$_2$ activation with **6b**, the lack of reactivity with Cp complex **5b** is striking. It is compelling to suggest that the κ^3-(P,P,Ar) isomer contributes to the stability of **5b**, it is unlikely however that this is the only factor since the N$_2$ adduct is present in significant quantities at room temperature. More likely, the Cp* ligand gives a sufficiently electron rich metal to achieve C–Cl activation. The facile formation of complex **7** reveals the sensitivity of catalyst **6b** to side reactions, particularly with alkyl halides.

Lifetime of Active Catalysts 5b and 6b

Catalytic intramolecular hydroamination of **EA** was conducted with the Cp and Cp* active complexes **5b** and **6b**, respectively (Scheme 4). For an additional comparison, the chloro complex **3b** was included that requires halide dissociation to enter the catalytic cycle. Reactions were conducted under standard conditions of 0.1 mol% loading for 24 h at 70 °C and nitromethane was used to ensure complete solubility of the catalysts. The data below are compared to TON values for **1b**/**2b** in Me-THF, but control reactions indicated that the nature of the solvent does not influence the TON values.

At 70 °C the TONs for the active complexes **5b** and **6b** are 220 and 160, respectively (Figure 11). The ca. 1.4-fold higher lifetime of the Cp catalyst is consistent with the relative values for the pre-catalyst analogues **1b** and **2b**. However, the magnitude of the difference is smaller than would be expected

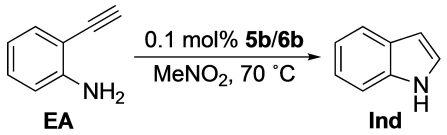

Scheme 4. Benchmark cyclization of **EA** to indole catalyzed using the coordinatively unsaturated complexes **5b** and **6b**, and a control reaction with the complex **3b**.

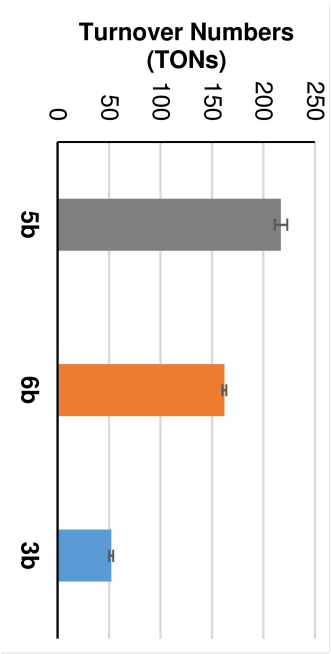

Figure 11. TON comparison with 0.1 mol% of donor-free complexes **5 b** and **6 b**, and chloro complex **3 b** toward the intramolecular hydroamination of **EA** at 70 °C, in CH_3NO_2. TONs were determined after 24 h by GC-FID analysis. Runs were conducted in duplicate with data points representing the average and the error bars depict the span of individual runs.

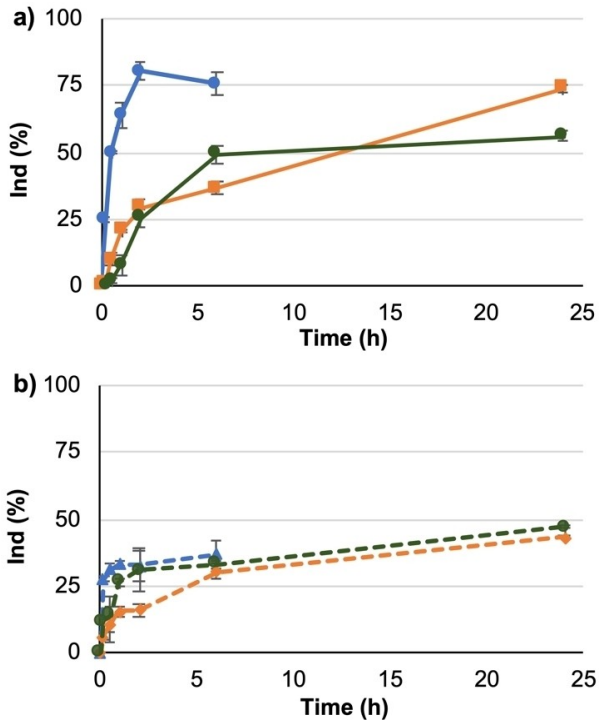

Figure 12. Reaction profiles for the intramolecular hydroamination of **EA** with a) Cp complexes **1 a–c** (solid lines); and b) Cp* complexes **2 a–c** (dashed lines). Conditions: 300 mM **EA**, Me-THF, 70 °C, 0.1 mol% [Ru]; **1 a** (blue), **1 b** (orange), **1 c** (green), **2 a** (blue), **2 b** (orange), **2 c** (green). Runs were conducted in duplicate with data points representing the average and the error bars depict the span of individual runs.

based on thermal stability, in which **5 b** is ca. seven-fold more stable than **6 b**. This suggests that coordination of the substrate and/or product to ruthenium offers some degree of protection from decomposition, which may be particularly important for the Cp* analogue that does not benefit from $P^{Cy}_2N^{Ph}_2$ hemilability for stability. The TONs of the active catalysts **5 b** and **6 b** are ca. three times lower than their corresponding pre-catalysts **1 b** and **2 b**, respectively. Despite the facile initiation of the pre-catalysts to the active catalysts at 70 °C, the equilibrium binding of acetonitrile still offers notable stabilization. The low lability of the chloro ligand in **3 b**, even at elevated temperature in the relatively polar nitromethane solvent, leads to a poor TON of only 50. Previously, we found that pre-catalysts **1 a**/**2 a** exhibited poor performance at 40 °C due to slow conscription into the catalytic cycle via MeCN dissociation. Since this step is precluded with the active catalysts **5 b** and **6 b**, we anticipated high TONs could be achieved at room temperature. Unfortunately, no conversion was observed for **5 b**, which indicates that an on-cycle step in the catalytic mechanism has a sufficiently high barrier to prevent catalysis at this temperature.

Reaction Rate Comparison of Catalysts 1 a-c and 2 a-c

Hydroamination of **EA** under standard conditions with catalysts **1 a–c** and **2 a–c** (Scheme 1) was monitored over time by GC-FID (Figure 12). Turnover frequencies, calculated at 50 % of the maximum conversion, of 1300, 60, and 110 h^{-1} for **1 a**, **1 b**, and **1 c**, respectively, revealed that the R = *t*-Bu catalyst is much faster than the R = Cy or Ph derivatives. The TOF of the donor-free complex **5 b** is ca. 10 h^{-1} (Figure S58), which may suggest that the κ^3-(P,P,Ar) coordination mode slows catalysis. However, MeCN readily displaces the π-arene interaction, therefore the slow rate may be due to competitive binding of the amine of **EA**. The TOFs for **2 a-c** of 1530, 1330 and 200 h^{-};[1], respectively, show that in all cases the Cp* derivatives are faster than the Cp analogues. This is consistent with the prior study of **1 a** and **2 a**,[8c] and this confirms the trend is general to other catalyst derivatives. The difference in rate between Cp and Cp* complexes is likely a consequence of conscription of the pre-catalyst to the κ^2-(P,P) active catalyst. This species is likely more prevalent with all Cp* derivatives due to higher MeCN lability.

Product Inhibition of Catalyst 1 b

A qualitative comparison of the reaction profiles (Figure 12) reveals that conversion rates with the R = Cy catalysts **1 b** and **2 b** slow down considerably after ca. 20 % conversion of **EA**. This attenuation suggests that the indole (**Ind**) product may inhibit catalysis. To evaluate this, Variable Time Normalization Analysis (VTNA)[23] was employed by examining **EA** consumption over time (Figure 13). Hydroamination was conducted with a consistent concentration of **1 b** and two different concentrations of **EA** (Run A = 150 and Run B = 100 mM). The starting

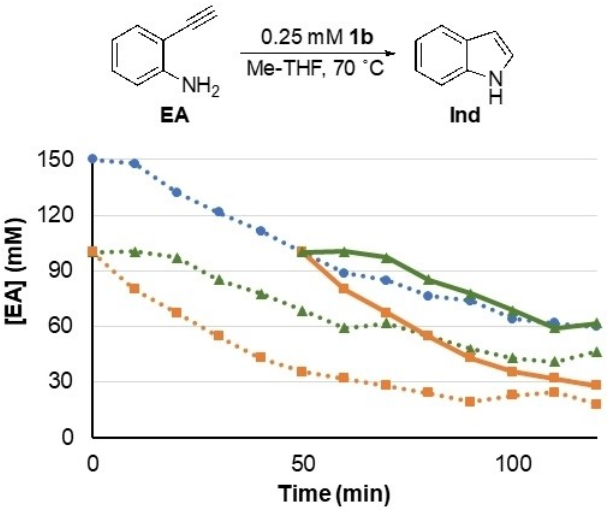

Figure 13. (top) Intramolecular hydroamination of **EA** with catalyst **1 b** (0.25 mM) to form **Ind**. (bottom) Reaction profiles for runs with initial concentrations of: A, 150 mM **EA** (●, blue); B, 100 mM **EA** (■, orange); and C 100 mM **EA** and 50 mM **Ind** (▲, green) Solid lines (–) are time-shifted (Run B = orange; Run C = green). Reactions were performed in duplicate and in all cases the error was within ± 5 %.

substrate concentration of Run B corresponds to the amount of **EA** remaining after 34 % conversion of Run A, which is observed after 50 min. The Run B data was shifted along the time axis so that the first data point aligned with the 50 min data point of Run A. The two lines should overlap if catalyst inhibition is negligible. In this case, Run A and time-shifted Run B data do not overlap and the latter exhibits faster consumption of **EA**. A third set of conditions (Run C) was completed with 100 mM **EA** and 50 mM **Ind**, which corresponds the actual speciation in Run A after 50 min. The data for Run C and A are in close agreement, which indicates that the presence of **Ind** attenuates consumption of **EA** due to catalyst inhibition. Given that product formation is not completely arrested, the inhibition process negatively affects only the catalytic rate rather than overall TONs. In fact, as suggested above the **Ind** adduct (**Ru-Ind**) may offer some catalyst stabilization.

Catalyst inhibition would result from competitive coordination of either the heterocyclic π-bond or the nitrogen lone pair of indole to the catalyst active site (e.g. **Ru-Ind** in Scheme 5). Regeneration of the active catalyst would rely on the lability of bound indole. A related κ^1-(N) pyrrolidine adduct, [Ru-(Cp)($P^{Ph}{}_2N^{Bn}{}_2$)(pyrr)]PF_6, was previously characterized, and in the solid-state it exhibited a hydrogen bond between the Lewis base and the proximal pendent amine of the ligand.[24] Treatment of **5 b** with 200 equiv. **Ind** resulted in an immediate colour change from dark red to yellow, which is typical for coordinatively-saturated complexes of the type [Ru(Cp/Cp*)($P^R{}_2N^{R'}{}_2$)(L)]PF_6.[8,10, 24] Formation of a single new species was not observed. Rather, the $^{31}P\{^1H\}$ NMR signals for the two isomers of **5 b** were both shifted downfield by ca. 4 ppm, consistent with equilibrium binding of **Ind** that favors the active complex structures. In line with this observation, attempts to isolate the **Ru-Ind** adduct were unsuccessful. While the formation of **Ru-Ind** suppresses the catalytic rate the adduct may protect the active catalyst from decomposition as an off-cycle intermediate.

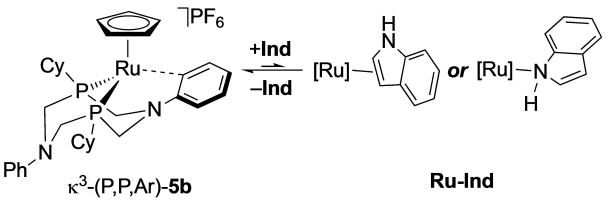

Scheme 5. Proposed equilibrium between **κ^3-(P,P,Ar)-5 b** and possible inhibition adducts **Ru-(κ^1-N-Ind)** and **Ru-(η^2-Ind)**. Note: samples of **5 b** also contain κ^2-(P,P) **5 b-N_2**. [Ru] = [Ru(Cp)($P^{Cy}{}_2N^{Ph}{}_2$)]PF_6.

Substrate Modification to Avoid Product Inhibition of Catalyst 1 b

We considered that simple modification of the primary amine substrate to a secondary amine, such as 2-ethynyl-*N*-methylaniline (**Me-EA**), could prevent catalyst inhibition. VTNA with **1 b** and **Me-EA** was conducted following a similar set of three Runs A–C (Figure 14) that were described above with **EA**. A 50 mM substrate concentration was used for Run A and 35 mM was used for Runs B and C, which corresponded to the amount of **EA** at a reaction time of 30 min in Run A. Run C also included 15 mM **Me-Ind** to directly mimic the speciation of Run A at t = 30 min. A shift in Run B and C data along the time axis shows that all three data sets overlap, which demonstrates that **Me-Ind** does not inhibit catalyst **1 b**. The lack of inhibition could be a consequence of the higher catalyst loading (3 mol%) as compared to that employed above with **EA** (0.2 mol%). Indeed,

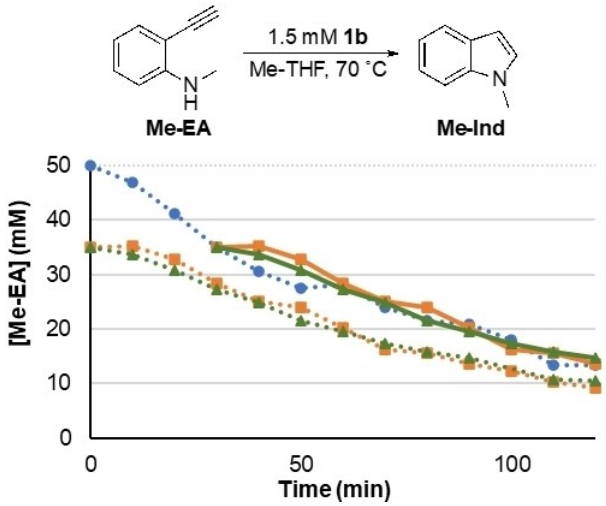

Figure 14. (top) Intramolecular hydroamination of **Me-EA** with catalyst **1 b** (1.5 mM) to form **Me-Ind**. (bottom) Reaction profiles for runs with initial concentrations of: A, 50 mM **Me-EA** (●, blue); B, 35 mM **EA** (■, orange); and C 35 mM **Me-EA** and 15 mM **Me-Ind** (▲, green) Solid lines (–) are time-shifted (Run B = orange; Run C = green). Reactions were performed in duplicate and in all cases the error was within ± 5 %.

catalysis with **EA** under conditions analogous to those used with **Me–Ind** did not lead to inhibition of catalyst **1 b** (SI, Figure S57). Adduct formation was instead evaluated by treatment of donor-free complex **5 b** with 200 equiv. of **Me-Ind**. No change in the $^{31}P\{^1H\}$ NMR resonances of **5 b** were observed, nor was there a color change from dark red that would support formation of an adduct. This is contrast to the analogous reaction with **Ind** that exhibits both spectroscopic and qualitative color changes indicative of **Ru-Ind** (*vide supra*). Thus, coordination of **Me–Ind** to the active catalyst **5 b** is suppressed as compared to **Ind** and this could be a consequence of the increased steric clash imposed by the methyl group, lower Lewis basicity, and/or lack of hydrogen bonding capability.

Conclusion

The catalytic lifetime and rate were assessed for a family of $[Ru(Cp/Cp^*)(P^R{}_2N^{Ph}{}_2)(MeCN)]PF_6$ complexes (R = *t*-Bu, Cy, Ph). The $P^{Cy}{}_2N^{Ph}{}_2$ ligand in the donor-free 'active' complex $[Ru(Cp)(P^{Cy}{}_2N^{Ph}{}_2)(MeCN)]PF_6$ coordinates to the metal through either a bidentate or tridentate mode. The latter involves coordination of ruthenium to the π-system of the N–Ph substituent, which increases the thermal stability of the Cp active catalyst by seven-fold over the Cp* analogue. Steric clash of the N-phenyl substituent with the methyl groups of Cp* likely precludes $P^{Cy}{}_2N^{Ph}{}_2$ hemilability in these derivatives. While the Cp derivatives have higher lifetimes, the catalytic rates are slower than the Cp* analogues. The attenuated rates of the Cp derivatives are not likely due to the κ^3-(P,P,Ar) coordination mode, since the stabilizing interaction is readily displaced by a donor molecule (e.g., MeCN). Rather, the rate is most sensitive to catalyst inhibition by the hydroamination product **Ind**. Despite the attenuated rate, product coordination likely enhances turnover numbers by stabilizing the active catalyst. Therefore, the lifetime of catalyst **1 b** benefits from both intrinsic ($P^{Cy}{}_2N^{Ph}{}_2$ hemilability) and extrinsic (reversible MeCN/**Ind** coordination) factors. This study shows that with Ru(Cp) complexes the $P^R{}_2N^{Ph}{}_2$ ligand displays two beneficial types of metal-ligand cooperativity: proton-transfer via the pendent tertiary amines, which avoids basic additives; and a change in ligand coordination to stabilize the low-coordinate active catalyst.

Experimental Section

All reactions were carried out under an inert atmosphere of Ar or N_2 using standard Schlenk or glovebox techniques, respectively, unless otherwise stated. All glassware was oven dried (150 °C) prior to use. All chemicals were obtained from Sigma-Aldrich, Alfa Aesar, or Oakwood, and used without further purification unless otherwise stated. $CDCl_3$ (99.8 %), DCM-d_2, and acetone-d_6, were obtained from Cambridge Isotope Laboratories. $P^{Cy}{}_2N^{Ph}{}_2$,[25] $[RuCl(Cp^*)(PPh_3)_2]$,[26] $[Ru(Cp)(P^{t-Bu}{}_2N^{Ph}{}_2)(MeCN)]PF_6$ (**1 a**),[8c] $[Ru(Cp)(P^{t-Bu}{}_2N^{Ph}{}_2)(MeCN)]PF_6$ (**1 c**),[8c] and $[Ru(Cp^*)(P^{t-Bu}{}_2N^{Ph}{}_2)(MeCN)]PF_6$ (**2 a**)[8c] were synthesized following literature procedures and the ^1H and $^{31}P\{^1H\}$ spectroscopic data matched literature values. Dry and degassed tetrahydrofuran (THF), diethyl ether (Et_2O), and acetonitrile (MeCN) were obtained from an Innovative Technology 400–5 Solvent purification system and stored under N_2. These dry and degassed solvents, aside from MeCN, were stored over 4 Å molecular sieves, while MeCN was stored over 3 Å molecular sieves (Fluka and activated at 150 °C in an oven). Absolute ethanol was degassed by bubbling with argon. 2-methyltetrahydrofuran (Me-THF), fluorobenzene, nitromethane, deuterated nitromethane, and $CDCl_3$ were dried using 4 Å molecular sieves and degassed by bubbling with argon.

Charge-transfer Matrix Assisted Laser Desorption/Ionization (MALDI) mass spectrometry data were collected on an AB Sciex 5800 TOF/TOF mass spectrometer using pyrene as the matrix in a 20:1 molar ratio to metal complex. Samples were spotted on the target plate as solutions in CH_2Cl_2. NMR spectra were acquired on an either an INOVA 400 or 600 MHz, or a Bruker 400 MHz NMR spectrometer. ^1H NMR spectra acquired were referenced internally against the residual protio-solvent signal to tetramethylsilane at 0 ppm and $^{13}C\{^1H\}$ NMR spectra were referenced internally against the solvent signal to tetramethylsilane at 0 ppm. $^{31}P\{^1H\}$ spectra were referenced externally to 85 % phosphoric acid at 0.00 ppm. Infrared spectra were collected on solid samples using a PerkinElmer UATR TWO FTIR spectrometer. Quantification of catalytic conversion of **EA**, **Ind**, and **Me–Ind**, were achieved using an Agilent 7890a gas chromatography with a flame ionization detector (GC-FID), fitted with a HP-5 column, unless otherwise stated. Calibration curves for **EA**, **Ind**, and **Me–Ind**, were prepared to determine the response factor. The amount of each species was quantified, relative to the internal standard (tetralin), using area counts corrected with the response factor.

General Procedure for Synthesis of Pre-Catalysts $[Ru(Cp)(P^R{}_2N^{R'}{}_2)(MeCN)][PF_6]$ (1 b, 2 b, 2 c). A 100 mL Schlenk flask was charged with a stir bar, $[Ru(Cp)(MeCN)_3][PF_6]$ or $[Ru(Cp^*)(MeCN)_3][PF_6]$ (0.21–0.26 mmol, 1 equiv), ligand $P^{Cy}{}_2N^{Ph}{}_2$ or $P^{Ph}{}_2N^{Ph}{}_2$ (0.23–0.27 mmol, 1.05 equiv, and MeCN/DCM (12 mL, 1:1). The flask was heated under a flow of argon at 35 °C for 1 h, the solvent was removed *in vacuo*, and the flask with the remaining solid residue was transferred into a glovebox. The solid was dissolved in MeCN and the suspension was then filtered through a microfibre pipette filter to remove insoluble ligand. The solvent of the filtrate was removed *in vacuo* to give an orange/yellow solid, which was triturated and washed with diethyl ether (3 x 5 mL). The solid was further dried *in vacuo* to remove any residual solvent.

$[Ru(Cp)(P^{Cy}{}_2N^{Ph}{}_2)(MeCN)][PF_6]$ (1 b). Yield = 93 %. ^1H NMR (600 MHz, CD_2Cl_2): δ 7.36-7.25 (m, Ph-*H*, 4H), 7.05-7.00 (m, Ph-*H*, 2H), 6.99-6.94 (m, Ph-*H*, 1H), 6.91-6.86 (m, Ph-*H*, 3H), 4.83 (s, Cp-*H*, 5H), 3.83-3.75 (m, PCH_2N, 2H), 3.63-3.52 (m, PCH_2N, 4H), 3.52-3.46 (m, PCH_2N, 2H), 2.27-2.19 (m, Cy-*H*, 2H), 2.12 (s, $NCCH_3$, 3H), 2.11-2.03 (m, Cy-*H*, 2H), 2.03-1.80 (m, Cy-*H*, 8H), 1.63-1.25 (m, Cy-*H*, 10H). $^{13}C\{^1H\}$ NMR (151 MHz, CD_2Cl_2): δ 153.2 (t, $^3J_{C-P}$ = 6.9 Hz, C_{Ar}), δ 152.1 (t, $^3J_{C-P}$ = 6.0 Hz, C_{Ar}), 130.2 (C_{Ar}), 128.0 (C_{Ar}), 128.0 ($NCCH_3$), 122.1 (C_{Ar}), 121.2 (C_{Ar}), 118.3 (C_{Ar}), 117.3 (C_{Ar}), 80.5 (C_5H_5), 49.7 (X of ABX, N-CH_2-P), 46.9 (X portion of ABX spin system, N-CH_2-P), 42.1 (X of ABX, Cy), 28.8 (s, Cy), 28.5 (s, Cy), 27.5 (X of ABX, Cy), 27.1 (X of ABX, Cy), 26.6 (s, Cy), 4.4 (s, NC-CH_3). $^{31}P\{^1H\}$ NMR (162 MHz, CD_2Cl_2): δ 45.9 (s, Ru-*P*), −144.2 (sept, $^1J_{P-F}$ = 710.0 Hz). IR (neat) ν(cm^{-1}) 2924 (m), 2850 (m), 1595 (m), 1493 (m), 1201 (m), 835 (s), 749 (m), 692 (m), 556 (m). MALDI MS (pyrene matrix): Calc. *m/z* = 633.2 $[Ru(Cp^*)(P_2{}^{Cy}N_2{}^{Ph})]^+$, Obs. *m/z* = 633.2.

$[Ru(Cp^*)(P^{Cy}{}_2N^{Ph}{}_2)(MeCN)][PF_6]$ (2 b). Yield = 90 %. ^1H NMR (600 MHz, CD_2Cl_2): δ 7.34-7.27 (m, Ph-*H*, 4H), 7.07-6.99 (m, Ph-*H*, 4H), 6.99-6.92 (m, Ph-*H*, 2H), 3.90-3.83 (m, PCH_2N, 2H), 3.68-3.62 (m, PCH_2N, 2H), 3.27-3.17 (m, PCH_2N, 4H), 2.35 (s, $NCCH_3$, 3H), 1.74 (t, $^4J_{H-P}$ = 1.5 Hz, $C_5(CH_3)_5$, 15H), 2.21-1.80 (m, Cy-*H*, 12H), 1.59-1.25 (m, Cy-*H*, 8H). $^{13}C\{^1H\}$ NMR (151 MHz, CD_2Cl_2): δ 153.3 (t, $^3J_{C-P}$ = 7.2 Hz, C_{Ar}), 152.2 (t, $^3J_{C-P}$ = 9.7 Hz, C_{Ar}), 129.5 (C_{Ar}), 129.4 (C_{Ar}), 126.0 ($NCCH_3$),

121.9 (C_{Ar}), 121.0 (C_{Ar}), 118.4 (C_{Ar}), 116.8 (C_{Ar}), 92.1 ($C_5(CH_3)_5$), 45.8 (X of ABX, N-CH_2-P), 45.1 (X of ABX, N-CH_2-P), 39.4 (X of ABX, Cy), 27.6 (Cy), 27.3 (X of ABX, Cy), 27.0 (X of ABX, Cy), 26.9 (X of ABX, Cy), 26.1 (Cy), 10.2 ($C_5(CH_3)_5$), 4.2 (NC-CH_3). $^{31}P\{^1H\}$ NMR (243 MHz, CD_2Cl_2): δ 36.0 (s, Ru-*P*), −143.9 (sept, $^1J_{P-F}$ = 711.2 Hz). IR (neat) ν(cm^{-1}) 2919 (m), 2849 (m), 1655 (m), 1595 (s), 1492 (s), 1192 (s), 840 (s), 739 (m). MALDI MS (pyrene matrix): Calc. *m/z* = 703.3 [Ru(Cp*)($P_2^{Cy}N_2^{Ph}$)]$^+$, Obs. *m/z* = 703.2.

[Ru(Cp*)($P^{Ph}_2N^{Ph}_2$)(MeCN)][PF_6] (2 c). Yield = 82 %. ^1H NMR (600 MHz, CD_2Cl_2): δ 7.71-7.58 (m, Ph-*H*, 11H), 7.45-7.38 (t, Ph-*H*, 1H), 7.29-7.20 (m, Ph-*H*, 4H), 7.09-7.04 (t, Ph-*H*, 1H), 6.90-6.83 (m, Ph-*H*, 3H), 4.12–4.02 (m, PCH_2N, 4H), 3.98-3.91 (m, PCH_2N, 2H), 3.88-3.81 (m, PCH_2N, 2H), 2.22 (s, CH_3CN, 3H), 1.36 (s, $C_5(CH_3)_5$, 15H). $^{13}C\{^1H\}$ NMR (151 MHz, CD_2Cl_2): δ 153.7 (t, $^3J_{C-P}$ = 6.9 Hz, C_{Ar}), 151.8 (t, $^3J_{C-P}$ = 6.0 Hz, C_{Ar}), 132.2 (X of ABX, C_{Ar}), 131.6 (C_{Ar}), 130.9 (X of ABX, C_{Ar}), 130.2 (C_{Ar}), 130.2 (C_{Ar}), 130.1 (X of ABX, C_{Ar}), 127.7 (NCCH_3), 122.8 (C_{Ar}), 121.1 (C_{Ar}), 119.0 (C_{Ar}), 117.4 (s, C_{Ar}), 93.9 ($C_5(CH_3)_5$), 53.3 (X of ABX, N-CH_2-P), 48.4 (X of ABX, N-CH_2-P), 10.1 ($C_5(CH_3)_3$), 4.6 (NC-CH_3). $^{31}P\{^1H\}$ NMR (162 MHz, CD_2Cl_2): δ 31.0 (s, Ru-*P*), −144.2 (sept, $^1J_{P-F}$ = 710.0 Hz). IR (neat) ν(cm^{-1}) 3058 (vs), 2896 (w), 2847 (w), 1659 (m), 1594 (m), 1189 (m), 832 (s), 691 (m), 556 (m). MALDI MS (pyrene matrix): Calc. *m/z* = 691.2 [Ru(Cp*)($P_2^{Cy}N_2^{Ph}$)]$^+$, Obs. *m/z* = 691.1.

General Procedure for [RuCl(Cp/Cp*)($P^{Cy}_2N^{Ph}_2$)] Complex Synthesis. A 100 mL Schlenk flask was charge with a stir bar, [RuCl(Cp)(PPh_3)$_2$] (0.12 mmol, 1 equiv) or [RuCl(Cp*)(PPh_3)$_2$] (0.12 mmol, 1 equiv), $P^{Cy}_2N^{Ph}_2$ ligand (0.12 mmol, 1 equiv), and toluene (20 mL). The flask was refluxed under a flow of argon for 72 h and a colour change from orange to yellow was observed. The solvent was cooled to room temperature and then removed *in vacuo* resulting in a yellow oil. The oil was triturated with hexanes to give a yellow powder which was subsequently washed with hexanes (3 × 5 mL) and dried under reduced pressure.

[RuCl(Cp)($P^{Cy}_2N^{Ph}_2$)] (3 b). Yield = 86 %. ^1H NMR (600 MHz, CD_2Cl_2): δ 7.28-7.24 (m, Ph-*H*, 2H), 7.22-7.17 (m, Ph-*H*, 2H), 7.03-6.99 (m, Ph-*H*, 2H), 6.90-6.86 (m, Ph-*H*, 1H), 6.78-6.74 (m, Ph-*H*, 2H), 6.71-6.67 (m, Ph-*H*, 1H), 4.53 (s, Cp-*H*, 5H), 4.23-4.16 (m, PCH_2N, 2H), 3.74-3.69 (m, PCH_2N, 2H), 3.52-3.44 (m, PCH_2N, 2H), 3.39-3.33 (m, PCH_2N, 2H), 2.44-2.39 (m, Cy-*H*, 2H), 2.12-2.05 (m, Cy-*H*, 2H), 2.00-1.88 (m, Cy-*H*, 6H), 1.83-1.77 (m, Cy-*H*, 2H), 1.72-1.63 (m, Cy-*H*, 2H), 1.46-1.29 (m, Cy-*H*, 8H). $^{13}C\{^1H\}$ NMR (151 MHz, CD_2Cl_2): δ 154.2 (t, $^3J_{C-P}$ = 7.0 Hz, C_{Ar}), 150.9 (t, $^3J_{C-P}$ = 4.1 Hz, C_{Ar}), 129.3 (C_{Ar}), 129.2 (C_{Ar}), 120.4 (C_{Ar}), 117.9 (C_{Ar}), 117.8 (C_{Ar}), 114.4 (C_{Ar}), 77.6 (C_5H_5), 46.7 (X of ABX, N-CH_2-P), 43.6 (X of ABX, N-CH_2-P), 42.6 (X of ABX, Cy), 28.6 (Cy), 27.9 (Cy), 27.2 (X of ABX, Cy), 26.8 (X of ABX, Cy), 26.4 (Cy). $^{31}P\{^1H\}$ NMR (212 MHz, CD_2Cl_2): δ 46.6 (s, Ru-*P*). IR (neat) ν(cm^{-1}) 2923 (m), 2846 (m), 1596 (m), 1499 (m), 1204 (m), 913 (m), 729 (s), 691 (s). MALDI MS (pyrene matrix): Calc. *m/z* = 668.2 [RuCl(Cp)($P_2^{Cy}N^{Ph}_2$)]$^+$, Obs. *m/z* = 668.1.

[RuCl(Cp*)($P^{Cy}_2N^{Ph}_2$)] (4 b) Yield = 86 %. ^1H NMR (600 MHz, CD_2Cl_2): δ 7.27-7.16 (m, Ph-*H*, 4H), 7.03-6.97 (m, Ph-*H*, 2H), 6.96-6.91 (m, Ph-*H*, 2H), 6.83-6.77 (m, Ph-*H*, 2H), 4.08-4.00 (m, PCH_2N, 2H), 3.69-3.57 (m, PCH_2N, 4H), 3.10-3.03 (m, PCH_2N, 2H), 2.45-2.37 (m, Cy-*H*, 2H), 2.26-2.17 (m, Cy-*H*, 2H), 2.07-2.00 (m, Cy-*H*, 2H), 1.95-1.88 (m, Cy-*H*, 4H), 1.81-1.74 (m, Cy-*H*, 2H), 1.67 (s, $C_5(CH_3)_5$, 15H), 1.62-1.21 (m, Cy-*H*, 8H), 1.12-0.98 (m, Cy-*H*, 2H). $^{13}C\{^1H\}$ NMR (101 MHz, CD_2Cl_2): δ 154.9 (t, $^3J_{C-P}$ = 6.5 Hz, C_{Ar}), 153.7 (t, $^3J_{C-P}$ = 8.5 Hz, C_{Ar}), 129.7 (C_{Ar}), 120.5 (C_{Ar}), 119.8 (C_{Ar}), 118.0 (C_{Ar}), 116.2 (C_{Ar}), 89.7 ($C_5(CH_3)_5$), 46.0 (X of ABX, N-CH_2-P), 42.8 (X of ABX, N-CH_2-P), 41.4 (X of ABX, Cy), 28.6 (Cy), 27.9 (Cy), 27.2 (X of ABX, Cy), 28.4 (Cy), 28.1 (X of ABX, Cy), 27.9 4 (X of ABX, Cy), δ 27.1 (Cy). $^{31}P\{^1H\}$ NMR (162 MHz, CD_2Cl_2): δ 34.4 (Ru-*P*). IR (neat) ν(cm^{-1}) 2914 (m), 2848 (m), 1590 (m), 1501 (s), 1212 (m), 738 (s), 685 (s). MALDI MS (pyrene matrix): Calc. *m/z* = 738.3 [RuCl(Cp*)($P_2^{Cy}N_2^{Ph}$)]$^+$, Obs. *m/z* = 738.2.

General Procedure for [Ru(Cp/Cp*)($P^{Cy}_2N^{Ph}_2$)]PF_6 Complex Synthesis. $TlPF_6$ was used in this procedure. Thallium is extremely TOXIC and due care is needed.[27] Solid waste and solution waste contaminated with thallium were placed in a separate containers marked for thallium waste. Glassware contaminated with thallium were heated in water to dissolve residual thallium salts. A 4 mL vial was charged with [RuCl(Cp)($P^{Cy}_2N^{Ph}_2$)] (0.010–0.011 mmol, 1 eq) in DCM (3 mL) or [RuCl(Cp*)($P^{Cy}_2N^{Ph}_2$)] (0.010–0.011 mmol, 1 eq) in C_6H_5F (3 mL) and $TlPF_6$ (0.011 mmol, 1.1 eq). The reaction was stirred for 2 h during which precipitation of a white solid, TlCl, and a distinct colour change from light yellow to red was observed. The suspension was filtered through a microfibre pipette filter to remove the precipitate followed by solvent removal under reduced pressure. Both complexes were isolated as red powders and stored under inert atmosphere.

[Ru(Cp)(κ^2-$P^{Cy}_2N^{Ph}_2$)(N_2)][PF_6] (5 b-N_2) and [Ru(Cp)(κ^3-$P^{Cy}_2N^{Ph}_2$)][PF_6] (κ^3-(P,P,Ar)-5 b). Yield = 82 %. IR (neat) ν(cm^{-1}) 2925 (w), 2851 (w), 1594 (w), 1492 (w), 1194 (w), 833 (s), 743 (m), 853 (m). MALDI MS (pyrene matrix): Calc. *m/z* = 633.21 [Ru(Cp*)($P_2^{Cy}N_2^{Ph}$)]$^+$, Obs. *m/z* = 633.2.

(5 b-N_2). Mixture of **5 b-N_2** and **κ^3-(P,P,Ar)-5 b**, signals identified via elimination of known **κ^3-(P,P,Ar)-5 b** signals. Integration of ^1H NMR inaccurate due to mixture of signal overlap. ^1H NMR (400 MHz, CD_3NO_2): δ 7.17-7.07 (m, Ph-*H*, XH), 6.97-6.90 (m, Ph-*H*, XH), 6.86-6.81 (m, Ph-*H*, XH), 6.67-6.61 (m, Ph-*H*, XH), 4.62 (C_5H_5, XH), 3.77-3.70 (m, PCH_2N, XH), 3.64-3.60 (m, PCH_2N, XH), 3.34-3.28 (m, PCH_2N, XH), 2.41-2.20 (m, Cy-*H*, XH), 1.96-1.80 (m, Cy-*H*, XH), 1.72-1.66 (m, Cy-*H*, XH), 1.44-1.25 (m, Cy-*H*, XH). $^{13}C\{^1H\}$ NMR (151 MHz, CD_2Cl_2): δ 155.4 (t, $^3J_{C-P}$ = 7.1 Hz, C_{Ar}), 152.7 (t, $^3J_{C-P}$ = 5.9 Hz, C_{Ar}), 134.5 (C_{Ar}), 130.8 (C_{Ar}), 130.7 (t, $^3J_{C-P}$ = 3.1 Hz, C_{Ar}), 120.2 (C_{Ar}), 119.3 (C_{Ar}), 119.0 (m, C_{Ar}) 116.7 (C_{Ar}), 115.6 (s, C_{Ar}), 81.4 (C_5H_5), 48.6 (X of ABX, N-CH_2-P), 45.5 (X of ABX, N-CH_2-P), 43.1 (X of ABX, Cy–*C*), 41.9 (X of ABX, Cy–*C*), 30.3 (Cy–*C*), 29.3 (Cy–*C*), 28.4 (X of ABX, Cy–*C*), 28.1 (X of ABX, Cy–*C*), 27.8 (X of ABX, Cy–*C*), 27.6 (Cy–*C*), 27.2 (Cy–*C*), 26.7 (Cy–*C*), 9.2 (C_5CH_3)$_5$. $^{31}P\{^1H\}$ NMR (162 MHz, CD_2Cl_2): δ 43.9 (Ru-*P*, κ^2-P,P), −144.7 (sept, $^1J_{P-F}$ = 708.0 Hz, PF_6).

(κ^3-(P,P,Ar)-5 b). ^1H NMR (400 MHz, CD_2Cl_2): δ 7.41-7.27 (m, Ph-*H*, 2H), 7.25-7.12 (m, Ph-*H*, 2H), 7.09-6.87 (m, Ph-*H*, 5H), 6.46-6.36 (m, Ph-*H*, 1H), 4.52 (C_5H_5, 5H), 4.17-4.06 (m, PCH_2N, 2H), 3.67-3.58 (m, PCH_2N, 2H), 3.47-3.35 (m, PCH_2N, 2H), 3.31-3.20 (m, PCH_2N, 2H), 2.27-2.15 (m, Cy–H, 4H), 2.06-1.93 (m, Cy–H, 8H), 1.90-1.78 (m, Cy–H, 4H), 1.52-1.43 (m, Cy–H, 8H), 1.38-1.33 (m, Cy–H, 2H). $^{13}C\{^1H\}$ NMR (101 MHz, CD_2Cl_2): δ 152.0 (C_{Ar}), 151.3 (C_{Ar}), 133.1 (C_{Ar}), 129.9 (C_{Ar}), 122.4 (C_{Ar}), 120.9 (C_{Ar}), 118.4 (C_{Ar}), 95.8 (C_{Ar}), 79.9 (C_5H_5), 55.6 (P-CH_2-N), 49.3 (P-CH_2-N), 40.7 (X of ABX, Cy), 29.1 (X of ABX, Cy), 27.0 (Cy), 25.9 (Cy), 18.8 (Cy). $^{31}P\{^1H\}$ NMR (162 MHz, CD_2Cl_2): δ 73.6 (s, Ru-*P*, κ^3-P,P,Ar), −144.2 (sept, $^1J_{P-F}$ = 708.0 Hz, PF_6).

[Ru(Cp*)($P^{Cy}_2N^{Ph}_2$)]PF_6 (6 b). Yield = 88 %. ^1H NMR (400 MHz, CD_3NO_2): δ 7.36-7.26 (m, Ph-*H*, 4H), 7.25-7.19 (m, Ph-*H*, 2H), 7.18-7.12 (m, Ph-*H*, 2H), 7.03-6.92 (m, Ph-*H*, 2H), 4.13-4.04 (m, PCH_2N, 2H), 3.96-3.88 (m, PCH_2N, 2H), 3.88-3.81 (m, PCH_2N, 2H), 3.53-3.41 (m, PCH_2N, 4H), 2.45-2.32 (m, Cy-*H*, 2H), 2.29-2.07 (m, Cy-*H*, 4H), 2.04-1.90 (m, Cy-*H*, 2H), 1.91 (t, $^4J_{H-P}$ = 1.56, $C_5(CH_3)_5$, 15H), 1.85-1.76 (m, Cy-*H*, 4H), 1.59-1.45 (m, Cy-*H*, 4H), 1.44-1.20 (m, Cy-*H*, 6H). $^{13}C\{^1H\}$ NMR (101 MHz, CD_3NO_2): δ 153.2 (t, $^3J_{C-P}$ = 7.9 Hz, C_{Ar}), 152.4 (t, $^3J_{C-P}$ = 9.9 Hz, C_{Ar}), 129.4 (C_{Ar}), 129.3 (C_{Ar}), 122.2 (C_{Ar}), 121.3 (C_{Ar}), 119.0 (C_{Ar}), 117.4 (C_{Ar}), 95.8 ($C_5(CH_3)_5$), 45.8 (X of ABX, N-CH_2-P), 45.5 (X of ABX, N-CH_2-P), 38.2 (X of ABX, Cy), 27.4 (Cy), 26.7 (X of ABX, Cy), 25.7 (X of ABX, Cy), 9.2 (C_5CH_3)$_5$. $^{31}P\{^1H\}$ NMR (162 MHz, CD_3NO_2): δ 33.5 (s, Ru-*P*), −144.2 (sept, $^1J_{P-F}$ = 706.2 Hz). IR (neat) ν(cm^{-1}) 2921 (w), 2580 (w), 1595 (m), 1492 (m), 1192 (m), 834 (vs), 752 (m), 595 (m). MALDI MS (pyrene matrix): Calc. *m/z* = 703.29 [Ru(Cp*)($P_2^{Cy}N_2^{Ph}$)]$^+$, Obs. *m/z* = 703.3.

General Procedure for [RuCl(Cp/Cp*)($P^{Cy}_2N^{Ph}_2$)] Halide Abstraction Under Argon Gas. $TlPF_6$ was used in this procedure. Thallium is extremely TOXIC and due care is needed.[27] Solid waste and solution waste contaminated with thallium were placed in a separate containers marked for thallium waste. Glassware contaminated with thallium were heated in water to dissolve residual thallium salts. A 100 mL Schlenk flask was charged with CH_2Cl_2 (10 mL) or C_6H_5F (10 mL) and degassed with Argon by bubbling Ar through a needle submerged in the solvent. A separate 100 mL Schlenk flask was charge with a stir bar, [RuCl(Cp)($P^{Cy}_2N^{Ph}_2$)] (0.033 mmol, 1 equiv) or [RuCl(Cp*)($P^{Cy}_2N^{Ph}_2$)] (0.033 mmol, 1 equiv), and $TlPF_6$ (0.080 mmol, 2.4 equiv). The flask charged with solid material was cycled with argon to ensure displacement of all N_2. Solvent was canula transferred to dissolve either [RuCl(Cp)($P^{Cy}_2N^{Ph}_2$)] (CH_2Cl_2) or [RuCl(Cp*)($P^{Cy}_2N^{Ph}_2$)] (C_6H_5F), both resulting in a yellow solution, and the reaction was allowed to procedure for 2 h at room temperature. After ca. 5 minutes white solids precipitated from solution. The solution was then canula transferred through a filter and the solvent removed *in vacuo* which resulted in a solid powder for both reactions.

Procedure for [RuCl(η^4-$C_5Me_5CH_2Cl$)($P^{Cy}_2N^{Ph}_2$)][PF_6] Complex Synthesis. A 20 mL vial was charged with [Ru(Cp*)($P^{Cy}_2N^{Ph}_2$)][PF_6] (38 mg, 0.045 mmol, 1 eq) in DCM (5 mL).The reaction was stirred for 1 h at 70 °C or for 18 h at room temperature during which a colour change from light red to dark red occurred. The solvent was removed under reduced pressure and the dark red solid was washed with pentane. The complex was isolated as a red powder and stored under inert atmosphere.

[RuCl(η^4-($C_5Me_5CH_2Cl$))($P^{Cy}_2N^{Ph}_2$)][PF_6] (7). Yield = 90 %. ^{1}H NMR (600 MHz, CD_2Cl_2): δ 7.41-7.33 (m, Ph-*H*, 4H), 7.11-7.05 (m, Ph-*H*, 4H), 7.04-7.00 (m, Ph-*H*, 2H), 4.50-4.44 (m, PC*H*$_2$N, 1H), 4.24-4.19 (m, PC*H*$_2$N, 1H), 4.00-3.93 (m, PC*H*$_2$N, 1H), 3.64-3.57 (m, PC*H*$_2$N, 2H), 3.54 (d, $^2J_{H\text{-}H}$ = 11.2 Hz, $C_5(CH_2)_5CH_2Cl$, 1H), 3.50-3.42 (m, PC*H*$_2$N, 1H), 3.30-3.25 (d, $^2J_{H\text{-}H}$ = 11.2 Hz, $C_5(CH_2)_5CH_2Cl$, 1H), 3.24-3.19 (m, PC*H*$_2$N, 1H), 3.04-2.98 (m, PC*H*$_2$N, 1H), 2.67-2.58 (m, Cy-*H*, 1H), 2.45-2.38 (m, Cy-*H*, 1H), 2.38 (s, C(C*H*$_3$)CH_2Cl, 3H), 2.26-2.18 (m, Cy-*H*, 2H), 2.08-2.01 (m, Cy-*H*, 2H), 2.04 (s, C(C*H*$_3$)CH_2Cl, 3H), 1.98-1.90 (m, Cy-*H*, 4H), 1.97-1.84 (m, Cy-*H*, 1H), 1.82 (d, C_5*Me*$_5CH_2Cl$, 3H), 1.68-1.61 (m, Cy-*H*, 2H), 1.64 (s, C(C*H*$_3$)CH_2Cl, 3H), 1.52-1.45 (m, Cy-*H*, 2H), 1.39-1.28 (m, Cy-*H*, 6H), 1.17-1.07 (m, Cy-*H*, 1H), 0.80 (s, C(C*H*$_3$)CH_2Cl, 3H). $^{13}C\{^1H\}$ NMR (101 MHz, CD_2Cl_2): δ 152.8 (t, $^3J_{C\text{-}P}$ = 8.8 Hz, C_{Ar}), 150.8 (t, $^3J_{C\text{-}P}$ = 10.5 Hz, C_{Ar}), 130.5 (C_{Ar}), 130.3 (C_{Ar}), 129.3 (X of ABX, $C_5(CH_3)_5CH_2Cl$), 128.6 (X of ABX, $C_5(CH_3)_5CH_2Cl$), 124.2 (C_{Ar}), 123.2 (C_{Ar}), 120.0 (C_{Ar}), 117.5 (C_{Ar}), 104.0 ($C_5(CH_3)_5CH_2Cl$), 87.0 ($C_5(CH_3)_5CH_2Cl$), 53.0 (X of ABX, $C_5(CH_3)_5CH_2Cl$), 50.8 (X of ABX, $C_5(CH_3)_5CH_2Cl$), 47.9 (X of ABX, P-CH_2-P), 46.4 (X of ABX, P-CH_2-P), 44.6 (X of ABX, P-CH_2-P), 44.1 (X of ABX, P-CH_2-P), 40.2 (X of ABX, Cy), 37.8 (X of ABX, Cy), 28.9 (X of ABX, Cy), 28.6 (X of ABX, Cy), 28.1 (X of ABX, Cy), 27.9 (X of ABX, Cy), 27.4 (X of ABX, Cy), 27.3 (X of ABX, Cy), 26.9 (X of ABX, Cy), 26.3 (X of ABX, Cy), 13.2 ($C_5(CH_3)_5CH_2Cl$), 12.6 ($C_5(CH_3)_5CH_2Cl$), 12.0 ($C_5(CH_3)_5CH_2Cl$), 11.0 ($C_5(CH_3)_5CH_2Cl$), 1.3 ($C_5(CH_3)_5CH_2Cl$). $^{31}P\{^1H\}$ NMR (212 MHz, CD_2Cl_2): δ 71.9 (d, $^2J_{P\text{-}P}$ = 75.9 Hz, Ru-*P*), δ 31.8 (d, 75.9 Hz, Ru-*P*), −144.2 (sept, $^1J_{P\text{-}F}$ = 711 Hz, *P*F_6). IR (neat) ν(cm^{-1}) 2930 (w), 2851 (w), 1596 (w), 1492(w), 1192 (w), 832 (s), 556 (m). MALDI MS (pyrene matrix): Calc. *m/z* = 787.2 [RuCl(η^4-$C_5Me_5CH_2Cl$)($P^{Cy}_2N^{Ph}_2$)]$^+$ Obs. *m/z* = 784.2.

General Procedure for Intramolecular Hydroamination Catalysis. In a glovebox, the following stock solutions were prepared: **EA** (0.600 M) and tetralin (IS = internal standard) (0.400 M); **2a** (0.6 mM); **2b** (0.6 mM); **1c** (0.6 mM); **2c** (0.6 mM) all in Me-THF. Portions of substrate/IS stock solution (300 μL) and catalyst stock solution (300 μL) were dispensed into 4 mL screw cap reaction vials containing a stir bar. The final concentration for all reaction vials were 0.300 M in substrate, 0.200 M in tetralin (IS), and 0.3 mM in catalyst. A final 4 mL screw cap vial was charged with 100 μL of both substrate/IS stock solution and 100 μL Me-THF for use as the time = 0 sample, required for accurate quantification of substrate and product. The reaction vials were capped and removed from the glovebox and heated to 70 °C with stirring. After 0.167, 0.5, 1, 2, 6, and 24 h a vial was removed from heat, exposed to air, and a 20 μL aliquot was removed and diluted with 980 μL MeCN to quench the reaction. This diluted sample was subsequently analyzed by GC-FID. A 20 μL aliquot was also taken from the T0 sample and diluted with 980 μL of MeCN and analyzed by GC-FID. All catalytic runs were run in duplicate and each vial was injected three times and the area of the respective substrate, IS, and product peaks were averaged from the three injections.

General Catalytic Procedure for Product Inhibition Catalysis. In the glovebox, the following three stock solutions, **a**-**c** were prepared that contained: **EA** (**a** = 0.300 M, **b** = 0.200 M, **c** = 0.200 M), tetralin (**a** = 0.200 M, **b** = 0.135 M, **c** = 0.135 M), and **Ind** (**c** = 100 mM) in Me-THF. A catalyst stock solution was prepared with **1b** (0.5 mM) in Me-THF. Screw cap vials (4 mL) containing a stir bar were charged with catalyst stock solution (300 μL) and either substrate stock solution **a**, **b**, or **c** (300 μL). A total of 12 reactions vials were used for each reaction **A**, **B**, and **C** (total of 36 vials). The final concentration of the reaction vials were as follows: **A**) 150 mM **EA**, 100 mM IS, 0.25 mM **1b**, **B**) 100 mM **EA**, 68 mM IS, 0.25 mM **1b**, **C**) 100 mM **EA**, 68 mM IS, 0.25 mM **1b**, 50 mM **Ind**. Three 4 mL screw cap vials were charged with 100 μL of either stock solution **a**, **b**, or **c**, and 100 μL Me-THF for use as a time = 0 sample, required for accurate quantification of substrate and product. The vials were capped and removed from the glovebox and heated at 70 °C with stirring. A single reaction vial from each reaction **A**, **B**, and **C**, was removed from the heat every 10 minutes for 2 hours. Aliquots (20 μL) were taken from each reaction vial and diluted with 980 μL MeCN to quench the reaction. This diluted aliquot was subsequently analyzed by GC-FID. All catalytic runs were run in duplicate and each vial was injected three times and the area of the respective substrate, IS, and product peaks were averaged from the three injections.

General Procedure for Thermolysis of Complexes 1b, 2b, 5b, and 6b. An NMR tube was charged with a solution of complex **1b** (12 mg, 24 mM), **2b** (12 mg, 22 mM), **5b** (12 mg, 25 mM), or **6b** (12 mg, 24 mM) in CH_3NO_2. A sealed capillary containing the internal standard, $OPPh_3$, was added to the tube. For each sample, an initial (time = 0) $^{31}P\{^1H\}$ NMR spectrum was obtained at 25 °C. The samples were then heated at 70 °C in a mineral oil bath. The samples were periodically removed from the heat, cooled and $^{31}P\{^1H\}$ NMR spectra were obtained at 25 °C. The samples were heated for a total of 18 h and the relative integration of the starting complexes to internal standard were used to quantify decomposition of the complexes over time.

Acknowledgements

This work was financially supported by a Natural Sciences and Engineering Research Council (NSERC) of Canada Discovery Grant.

Conflict of Interest

The authors declare no conflict of interest.

Keywords: catalyst deactivation · hemilabile · heterocycles · ruthenium · structurally responsive ligands

[1] a) E. Vitaku, D. T. Smith, J. T. Njardarson, *J. Med. Chem.* **2014**, *57*, 10257–10274; b) T. C. Barden, in *Heterocyclic Scaffolds II:: Reactions and Applications of Indoles* (Ed.: G. W. Gribble), Springer Berlin Heidelberg, Berlin, Heidelberg, **2010**, pp. 31–46; c) J. Cossy, A. Guérinot, *Adv. Heterocycl. Chem., Vol. 119* (Eds.: E. F. V. Scriven, C. A. Ramsden), Academic Press, **2016**, pp. 107–142.
[2] a) J. A. Varela, C. González-Rodríguez, C. Saá, in *Ruthenium in Catalysis, Top. Organomet. Chem.* (Eds.: H. P. Dixneuf, C. Bruneau), Springer International Publishing, Berlin Heidelberg, **2014**, pp. 237–287; b) L.-H. Chung, C.-F. Yeung, C.-Y. Wong, *Chem. Eur. J.* **2020**, *26*, 6102–6112; c) L. Huang, M. Arndt, K. Gooßen, H. Heydt, L. J. Gooßen, *Chem. Rev.* **2015**, *115*, 2596–2697; d) T. E. Müller, K. C. Hultzsch, M. Yus, F. Foubelo, M. Tada, *Chem. Rev.* **2008**, *108*, 3795–3892.
[3] a) S. W. Roh, K. Choi, C. Lee, *Chem. Rev.* **2019**, *119*, 4293–4356; b) C. Bruneau, P. H. Dixneuf, *Acc. Chem. Res.* **1999**, *32*, 311–323.
[4] a) D. B. Grotjahn, *Top. Catal.* **2010**, *53*, 1009–1014; b) A. J. Arita, J. Cantada, D. B. Grotjahn, A. L. Cooksy, *Organometallics* **2013**, *32*, 6867–6870; c) A. A. Ogunlana, J. Zou, X. Bao, *J. Organomet. Chem.* **2018**, *864*, 160–168.
[5] a) B. M. Trost, Y. H. Rhee, *J. Am. Chem. Soc.* **2002**, *124*, 2528–2533; b) A. Varela-Fernández, A. Varela Jesús, C. Saá, *Adv. Synth. Catal.* **2011**, *353*, 1933–1937; c) A. Varela-Fernández, C. González-Rodríguez, J. A. Varela, L. Castedo, C. Saá, *Org. Lett.* **2009**, *11*, 5350–5353.
[6] a) R. H. Crabtree, *New J. Chem.* **2011**, *35*, 18–23; b) V. T. Annibale, D. Song, *RSC Adv.* **2013**, *3*, 11432–11449.
[7] a) R. N. Nair, P. J. Lee, D. B. Grotjahn, *Top. Catal.* **2010**, *53*, 1045–1047; b) R. N. Nair, P. J. Lee, A. L. Rheingold, D. B. Grotjahn, *Chem. Eur. J.* **2010**, *16*, 7992–7995.
[8] a) J. M. Stubbs, D. E. Chapple, P. D. Boyle, J. M. Blacquiere, *ChemCatChem* **2018**, *10*, 4001–4009; b) J. M. Stubbs, J. P. J. Bow, R. J. Hazlehurst, J. M. Blacquiere, *Dalton Trans.* **2016**, *45*, 17100–17103; c) J. M. Stubbs, B. J. Bridge, J. M. Blacquiere, *Dalton Trans.* **2019**, *48*, 7928–7937.
[9] J.-P. J. Bow, P. D. Boyle, J. M. Blacquiere, *Eur. J. Inorg. Chem.* **2015**, *2015*, 4162–4166.
[10] P. Bhattacharya, Z. M. Heiden, G. M. Chambers, S. I. Johnson, R. M. Bullock, M. T. Mock, *Angew. Chem. Int. Ed.* **2019**, *58*, 11618–11624; *Angew. Chem.* **2019**, *131*, 11744–11750.
[11] a) E. B. Hulley, N. Kumar, S. Raugei, R. M. Bullock, *ACS Catal.* **2015**, *5*, 6838–6847; b) E. B. Hulley, M. L. Helm, R. M. Bullock, *Chem. Sci.* **2014**, *5*, 4729–4741; c) S. Zhang, A. M. Appel, R. M. Bullock, *J. Am. Chem. Soc.* **2017**, *139*, 7376–7387; d) M. T. Mock, S. Chen, R. Rousseau, M. J. O'Hagan, W. G. Dougherty, W. S. Kassel, D. L. DuBois, R. M. Bullock, *Chem. Commun.* **2011**, *47*, 12212–12214; e) C. M. Klug, M. O'Hagan, R. M. Bullock, A. M. Appel, E. S. Wiedner, *Organometallics* **2017**, *36*, 2275–2284.
[12] J. M. Blacquiere, *ACS Catal.* **2021**, 5416–5437.
[13] H. Clavier, S. P. Nolan, *Chem. Commun.* **2010**, *46*, 841–861.
[14] Example prices of *t*-$BuPH_2$ (CAS: 2501–94-2) and $CyPH_2$ (CAS: 822–68-4) from Strem Chemicals, Inc., https://www.strem.com/catalog/v/15-0966/52/phosphorus 2501-94-2 and https://www.strem.com/catalog/v/15-0950/52/phosphorus 822-68-4, Accessed April 21, 2021
[15] a) M. Jiménez-Tenorio, M. C. Puerta, P. Valerga, *Eur. J. Inorg. Chem.* **2004**, *2004*, 17–32; b) T. J. Johnson, K. Folting, W. E. Streib, J. D. Martin, J. C. Huffman, S. A. Jackson, O. Eisenstein, K. G. Caulton, *Inorg. Chem.* **1995**, *34*, 488–499.
[16] a) A. D. Allen, C. V. Senoff, *Chem. Commun.* **1965**, 621–622; b) H. Aneetha, M. Jiménez-Tenorio, M. C. Puerta, P. Valerga, K. Mereiter, *Organometallics* **2002**, *21*, 628–635; c) J. M. Blacquiere, C. S. Higman, S. I. Gorelsky, N. J. Beach, S. J. Dalgarno, D. E. Fogg, *Angew. Chem. Int. Ed.* **2011**, *50*, 916–919; *Angew. Chem.* **2011**, *123*, 946–949.
[17] P. E. Garrou, *Chem. Rev.* **1981**, *81*, 229–266.
[18] a) P. S. Pregosin, *Coord. Chem. Rev.* **2008**, *252*, 2156–2170; b) J. M. Blacquiere, C. S. Higman, R. McDonald, D. E. Fogg, *J. Am. Chem. Soc.* **2011**, *133*, 14054–14062; c) N. Feiken, P. S. Pregosin, G. Trabesinger, A. Albinati, G. L. Evoli, *Organometallics* **1997**, *16*, 5756–5762.
[19] a) B. T. Ingoglia, C. C. Wagen, S. L. Buchwald, *Tetrahedron* **2019**, *75*, 4199–4211; b) D. S. Surry, S. L. Buchwald, *Chem. Sci.* **2011**, *2*, 27–50; c) R. Martin, S. L. Buchwald, *Acc. Chem. Res.* **2008**, *41*, 1461–1473; d) T. E. Barder, M. R. Biscoe, S. L. Buchwald, *Organometallics* **2007**, *26*, 2183–2192.
[20] D. D. Pathak, H. Adams, N. A. Bailey, P. J. King, C. White, *J. Organomet. Chem.* **1994**, *479*, 237–245.
[21] a) J. Chang, R. G. Bergman, *J. Am. Chem. Soc.* **1987**, *109*, 4298–4304; b) D. Rondon, X.-D. He, B. Chaudret, *J. Organomet. Chem.* **1992**, *433*, C18-C21; c) Y.-H. Lo, H.-G. Chen, T. S. Kuo, *Dalton Trans.* **2011**, *40*, 2711–2715.
[22] a) T. Kochi, Y. Nomura, Z. Tang, Y. Ishii, Y. Mizobe, M. Hidai, *J. Chem. Soc. Dalton Trans.* **1999**, 2575–2582; b) K. Tanaka, Y. Kushi, K. Tsuge, K. Toyohara, T. Nishioka, K. Isobe, *Inorg. Chem.* **1998**, *37*, 120–126; c) M. Basato, A. Biffis, C. Tubaro, C. Graiff, A. Tiripicchio, *Dalton Trans.* **2004**, 4092–4093; d) Y. Matsuo, Y. Kuninobu, S. Ito, M. Sawamura, E. Nakamura, *Dalton Trans.* **2014**, *43*, 7407–7412.
[23] a) J. Burés, *Angew. Chem. Int. Ed.* **2016**, *55*, 16084–16087; *Angew. Chem.* **2016**, *128*, 16318–16321; b) C. D. T. Nielsen, J. Burés, *Chem. Sci.* **2019**, *10*, 348–353.
[24] J. M. Stubbs, R. J. Hazlehurst, P. D. Boyle, J. M. Blacquiere, *Organometallics* **2017**, *36*, 1692–1698.
[25] A. Orthaber, M. Karnahl, S. Tschierlei, D. Streich, M. Stein, S. Ott, *Dalton Trans.* **2014**, *43*, 4537–4549.
[26] J. Yang, S. Langis-Barsetti, H. C. Parkin, R. McDonald, L. Rosenberg, *Organometallics* **2019**, *38*, 3257–3266.
[27] S. Galván-Arzate, A. Santamaría, *Toxicol. Lett.* **1998**, *99*, 1–13.

Manuscript received: July 9, 2021
Revised manuscript received: June 23, 2021
Version of record online: [redacted], [redacted]

FULL PAPERS

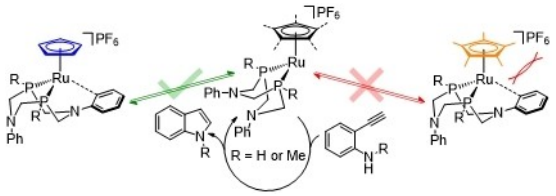

*D. E. Chapple, Dr. P. D. Boyle, Prof. J. M. Blacquiere**

Longer lifetimes: [Ru(Cp/Cp*)($P^{R}_{2}N^{R'}_{2}$)(MeCN)][PF_6] derivatives are active catalysts for the intramolecular hydroamination of alkynes. Evaluation of operationally unsaturated active catalysts revealed that the ability of the $P^{Cy}_{2}N^{Ph}_{2}$ ligand to switch from κ^2-(P,P) to κ^3-(P,P,Ar) stabilized the active catalyst to deactivation, which contributes to high lifetimes. VTNA analysis indicated product inhibition slows catalytic rates.